JOURNAL OF CATALYSIS 9, 154–165 (1967)

Kinetics and Mechanism in Catalytic Dehydrogenation of *n*-Butane over Chromia-Alumina

S. CARRÀ, L. FORNI, AND C. VINTANI

From the Istituto di Chimica Fisica, Università di Milano, Milano, Italy

Received February 28, 1967; revised July 3, 1967

The dehydrogenation reaction of *n*-butane over chromia-alumina has been kinetically investigated employing the differential reactor technique at temperatures ranging from 510° to 550°C. The runs were performed on *n*-butane and on mixtures of *n*-butane + 1-butene or *n*-butane + hydrogen, in the presence of an inert gas (nitrogen), with complete analysis of reaction products. The reaction rate data fit satisfactorily the dual-site mechanism.

A set of runs have been made on 10% chromia catalyst, containing different amounts of Li_2O or Na_2O. The progressive addition of Li_2O gave a continuous deactivation of the catalyst, while the progressive addition of Na_2O gave a deactivation followed by an activation. An interpretation of the reaction mechanism on the basis of electronic theory of catalysis is offered.

INTRODUCTION

The hydrocarbon dehydrogenation reactions are very important both from the scientific and the industrial points of view. Particularly the dehydrogenation of *n*-butane on solid catalysts is an important method for the preparation of butenes and butadiene. Apart from a considerable number of patents and technical publications, the first analysis of the kinetics of these reactions was performed by Dodd and Watson (*1*). Applying the integral reactor technique, these authors obtained a series of experimental data, which they interpreted on the basis of Langmuir-Hinshelwood theory. In their analysis they suggest that the kinetics of the process is controlled by the surface reaction, according to a dual-site mechanism.

In a more recent investigation (*2*) the reaction has been reexamined employing the differential reactor technique and both direct and reverse reactions have been tested. Nevertheless the results do not permit either confirmation of the dual-site mechanism, or suggestion of another one that could be accepted without reserve.

For that reason we considered that would be interesting to extend the kinetic researches on *n*-butane dehydrogenation, by means of the differential reactor technique over chromia-alumina catalysts. Furthermore the study has been extended to a series of catalysts containing small percentages of lithium oxide and sodium oxide in order to examine their influence on the catalyst activity.

EXPERIMENTAL

Materials

The *n*-butane and 1-butene were Phillips Petroleum Co. pure-grade products. Their purity, tested by gas chromatography, was superior to 99.5%, the remaining part being isobutane for the first product and *cis*- plus *trans*-2-butenes for the second one. Hydrogen and nitrogen were very high purity products (99.999%).

Catalysts

a. Materials. Alcoa F-110 ⅛-inch balls of alumina were used, with the following properties: Na_2O, 0.08%; surface area, 180–280 m^2/g; internal porosity, 0.272. Chro-

mium trioxide, sodium carbonate, and lithium carbonate were "reagent grade certified" products. Lithium carbonate was dried overnight at 0.01 mm Hg at a temperature of 57–58°C.

b. Preparations. The alumina was crushed and sieved; sizes between 20 and 40 mesh were separated and calcined in a tubular oven at 550°C with a small flow of dry nitrogen during 1 hr and kept dry.

The preparation of the catalysts was done following the method suggested by P. H. Emmett (*3*), by impregnating the alumina with solutions of CrO_3, or $CrO_3 + Na_2CO_3$, or $CrO_3 + Li_2CO_3$ in water, drying the

TABLE 1
PROPERTIES OF THE CATALYSTS

Type	Weight %			
	Al_2O_3	Cr_2O_3	Li_2O	Na_2O
00	100.0	—	—	—
0	90.0	10.0	—	—
1	89.5	10.0	0.5	—
2	89.0	10.0	1.0	—
4	88.0	10.0	2.0	—
5	89.5	10.0	—	0.5
6	89.0	10.0	—	1.0
8	88.0	10.0	—	2.0
9	80.0	20.0	—	—
14	95.0	5.0	—	—
17	85.0	15.0	—	—

impregnated solid at 150°C for 1 hr and then reducing it at 550°C for 1 hr with a small flow of dry hydrogen. After reduction the catalyst was cooled until its temperature was about 220°C with a small flow of dry nitrogen.

In Table 1 are listed the properties of the catalysts prepared and employed in experimental runs.

Equipment

The dehydrogenation runs were performed in a stainless steel (type 446) reactor, 2 cm in diameter, 50 cm in length, in which the catalyst was contained in a small basket, made of the same material, the bottom of which was formed of metal mesh. This reactor was heated by electrical resistances, placed in tubular refractory heaters surrounding the reactor. The temperature was controlled by means of an electronic regulating device, connected with four thermocouples: the first one was placed in the preheater, the second at the inlet point of the reactor, the third immediately above and the last one immediately below the catalytic bed. The temperature constancy was good (±1°C).

The flow diagram of the apparatus is given in Fig. 1. The *n*-butane, nitrogen, hydrogen, and 1-butene, taken from cylinders and metered by calibrated rotameters, were mixed and fed to the reactor. After

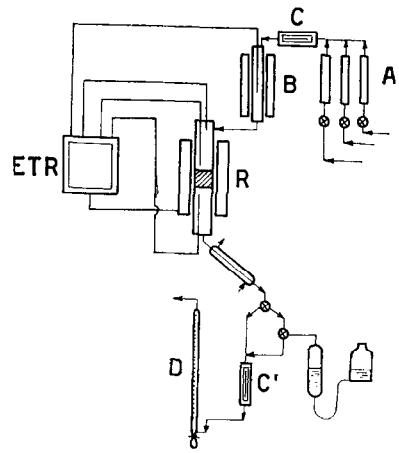

FIG. 1. Apparatus: A, rotameters; B, preheater; C, C', mercury thermometers; D, soap-bubble flow meter; R, reactor; ETR, electronic temperature regulator.

reaction the product gas was cooled by means of a double pipe heat exchanger and, by a suitable system of valves, it could be sent to a soap-bubble flow meter or to a sample collector. Temperatures of metered gases were taken by mercury thermometers inserted in the gas pipes.

Procedure

All runs were conducted with fresh catalyst as follows: After the weighed quantity of catalyst had been introduced into the catalyst basket, the reactor was stopped and flushed with a small nitrogen flow (50 ml/min) to eliminate oxygen. During this flushing, the reactor temperature was raised up to 100°C below the chosen reaction temperature and at this point we started the

feeding of the gas mixtures at the desired flow rates and ratios. One hour after starting the feeding of reacting gases the first sample of reaction gases was taken, controlling and recording all experimental conditions and data (temperature, flow rates, etc.). The second and the third samples were collected after 1.5 hr and 2 hr, respectively, and in the same way as the first one.

TABLE 2
TYPICAL RUN ANALYSIS

Temperature (°C)	520°
P_B (atm)	0.180
n-Butane feed rate (ml/min)	42.5
Nitrogen feed rate (ml/min)	195.5
Outgoing gas flow rate (ml/min)	253.5
n-Butane/nitrogen feed ratio	1/4.6
Catalyst type	4
Catalyst weight (g)	2.00
Outgoing gas analysis (% by vol)	
Nitrogen + hydrogen + methane	82.89
Ethane + ethylene	0.02
Propane	—
Propylene	0.04
n-Butane	16.74
1-Butene	0.05
trans-2-Butene	0.14
cis-2-Butene	0.10
Butadiene	0.02

The reaction rate was calculated by dividing the conversion by the time factor (W/F) W being the weight of the catalyst (g) and F the *n*-butane feed rate (moles/hr). The degree of reaction of *n*-butane was kept below 3%. In Table 2 a typical run analysis is given.

Analysis

The analysis of gases entering and leaving the reactor was done by gas chromatography, employing a Fractovap mod. B/f C.Erba thermal conductivity detector gas chromatograph. Satisfactory results have been obtained with a copper column, 4-mm ID and 8 m long, packed with 60–100 mesh activated alumina impregnated with propylene carbonate (21% by weight), and operated at the following conditions: column temperature, 15°C; carrier gas, hydrogen 10–30 ml/min; injected samples, 5 ml. The following components were determined: nitrogen + methane, ethane + ethylene, propane, propylene, isobutane, *n*-butane, 1-butene, *trans*-2-butene, *cis*-2-butene, butadiene.

RESULTS

A. Preliminary Runs

Some preliminary runs were done in order to select suitable values of the performance variables (temperature, pressure, flow rates) and of experimental conditions. A first set of runs, performed without any catalyst, showed that it was possible to operate up to the maximum temperature (550°C, at which the catalyst was calcined) with neither dehydrogenation nor cracking due to catalytic action of reactor internal surface. These runs have been done both with *n*-butane diluted with nitrogen and with pure *n*-butane, which flowed unaltered through the reactor even at 550°C and at the minimum flow rates employed in all following kinetic runs.

A second series of preliminary runs, performed with Type 0 catalyst, showed that the useful range of *n*-butane partial pressure was between 0.1 and 0.5 atm. Below 0.1 atm it was very difficult to make an accurate analysis of effluent gases, because of their excessive dilution in nitrogen; above 0.5 atm the cracking of *n*-butane became significant.

A third series of preliminary runs, with Type 00 catalyst, showed that, within the above-cited *n*-butane partial pressure limits, the catalytic action of pure alumina is negligible, even up to the maximum temperature of 550°C.

A last series of preliminary runs, performed with Type 0 catalyst at various *n*-butane partial pressures at 550°C, showed that the deactivation of the catalyst during the reaction time (about 2 hr) was negligible.

B. Experimental Data

A first series of experimental data have been collected in order to determine the kinetics of the reaction. All the runs of this series have been done with Type 0 catalyst at the temperatures of 550°, 530°, and 510°C. A set of runs has been made feeding

TABLE 3

EXPERIMENTAL RESULTS OF INITIAL RATE RUNS WITH TYPE 0 CATALYST[a]

T (°C)	P_B (atm)	r (moles/hr g cat.)	R (E)	R (C)	R (T)	R (D)
550°	0.111	0.0085	0.286	0.196	0.280	0.238
550°	0.125	0.0099	0.273	0.182	0.357	0.189
550°	0.143	0.0112	0.259	0.253	0.310	0.177
550°	0.143	0.0127	0.268	0.252	0.310	0.171
550°	0.181	0.0124	0.276	0.249	0.320	0.195
550°	0.181	0.0127	0.216	0.247	0.339	0.189
550°	0.181	0.0128	0.309	0.228	0.321	0.142
550°	0.200	0.0127	0.313	0.218	0.313	0.156
550°	0.250	0.0129	0.296	0.209	0.322	0.174
550°	0.303	0.0128	0.235	0.278	0.358	0.128
550°	0.333	0.0130	0.298	0.333	0.429	0.140
550°	0.400	0.0119	0.266	0.240	0.367	0.127
550°	0.500	0.0112	0.219	0.286	0.386	0.110
530°	0.111	0.0077	0.260	0.229	0.336	0.176
530°	0.143	0.0078	0.247	0.281	0.315	0.157
530°	0.181	0.0075	0.250	0.271	0.375	0.104
530°	0.250	0.0070	0.222	0.283	0.378	0.117
530°	0.303	0.0063	0.218	0.289	0.391	0.102
530°	0.375	0.0058	0.340	0.255	0.346	0.059
530°	0.425	0.0055	0.219	0.329	0.471	0.110
510°	0.111	0.0053	0.250	0.350	0.400	—
510°	0.150	0.0043	0.230	0.308	0.385	0.077
510°	0.181	0.0045	0.233	0.302	0.372	0.093
510°	0.250	0.0032	0.224	0.316	0.368	0.092
510°	0.333	0.0026	0.212	0.303	0.418	0.067
510°	0.387	0.0029	0.214	0.291	0.410	0.085
510°	0.500	0.0018	0.203	0.312	0.426	0.059

[a] The meaning of E, C, T and D appears in scheme (3); R is the ratio of each component to the sum of butenes plus butadiene.

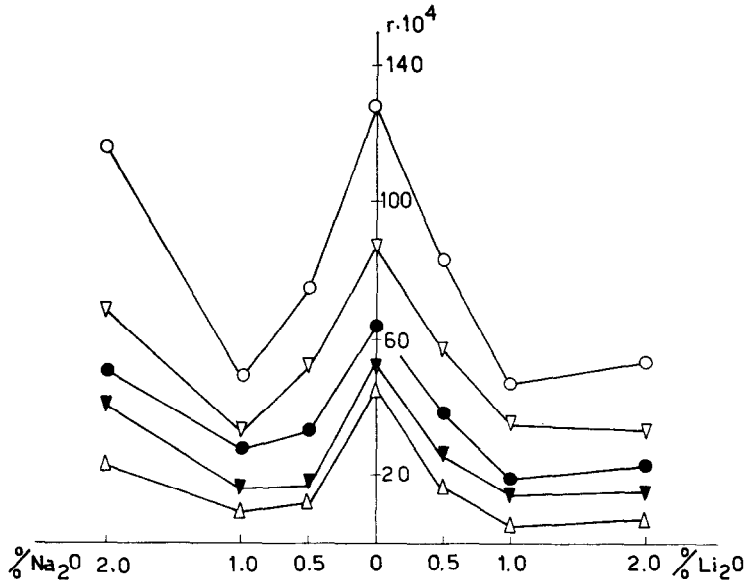

FIG. 2. Reaction rates (moles/hr g_c) vs. Na_2O or Li_2O percentages in the catalysts. Partial pressure of n-butane, 0.181 atm; ○, 550°C; ▽, 540°C; ●, 530°C; ▼, 520°C; △, 510°C.

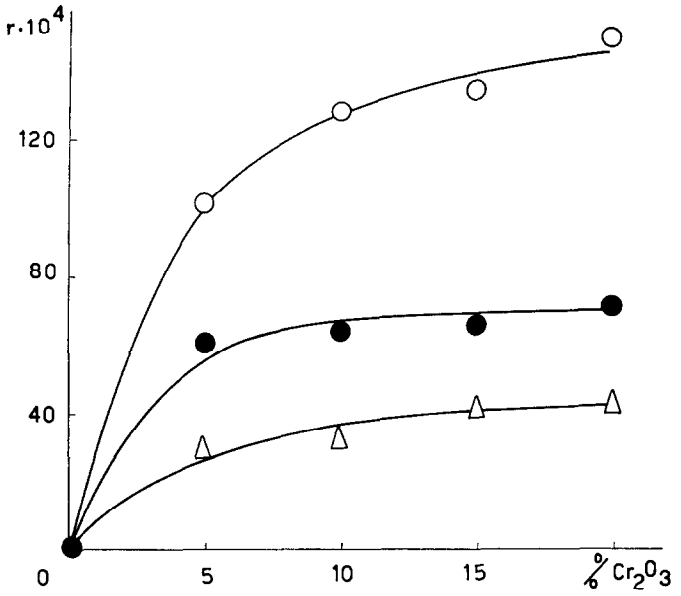

FIG. 3. Reaction rates (moles/hr g_c) vs. Cr_2O_3 percentages in the catalysts: ○, 550°C; ●, 530°C; △, 510°C.

only *n*-butane and nitrogen at various hydrocarbon partial pressures; the results are collected in Table 3. Four runs at each temperature were made feeding a mixture of *n*-butane, 1-butene, and nitrogen at various ratios of 1-butene to *n*-butane and at constant partial pressure of *n*-butane (0.181 atm). A similar set of runs was made feeding a mixture of *n*-butane, hydrogen, and nitrogen at various ratios of hydrogen to *n*-butane and at constant partial pressure of *n*-butane (0.181 atm).

With a second series of runs we tested the influence of the presence of various concentrations of Li_2O or Na_2O in the basic 10% chromia-on-alumina catalyst. These runs were performed at the temperatures of 550°, 540°, 530°, 520°, and 510°C and at the same *n*-butane partial pressure of 0.181 atm; values of reaction rates vs. Na_2O or Li_2O percentages are plotted in Fig. 2.

A third series of runs concerned the investigation of the influence on reaction rate of the chromia percentage on alumina, from 0% to 20%, without alkaline oxides. These data were collected at 550°, 530°, and 510°C and at the same *n*-butane partial pressure of 0.181 atm and are plotted in Fig. 3.

Reaction Kinetics

The influence of mass transfer on reaction kinetics has been tested by analyzing the values of the ratio $\Delta P_B/P_B$, where ΔP_B is the difference between the *n*-butane partial pressure in the gas stream (P_B) and at the surface of the catalyst particles, taken to be spherical, for some suitably chosen kinetic runs. Such a ratio is given by

$$\Delta P_B/P_B = (r/a_m k_g P_B \qquad (1)$$

where r is the reaction rate per unit mass of catalyst pellet, a_m the external area of pellets per unit mass of catalyst, k_{gB} the mass transfer coefficient of *n*-butane, calculated by means of the well known *J*-factor correlation (*4*). The diffusion coefficient of *n*-butane in nitrogen and the viscosity of the gas mixture have been evaluated applying the standard procedure (*5*). For the runs performed with Type 0 catalyst, the resulting values of $\Delta P_B/P_B$ were less than 0.01. Therefore the values of the partial pressure drops from gas stream to catalyst surface are quite small and the effect of external diffusion can be neglected.

A rough calculation, at the highest working temperature of 550°C, has been

made in order to evaluate the effect of diffusion of *n*-butane inside the catalyst particles on reaction kinetics. A mean value of the pore radius r_p of our catalyst particles, evaluated from pore volume and surface area data, was about 33 Å; the mean free path of *n*-butane at the reaction pressure is about 3.4×10^{-5} cm, that is, much greater than r_p. Therefore it is justified to assume that the internal diffusion is substantially Knudsen-type; the resulting effective diffusion coefficient, calculated with the known formula (*5*), is

$$D_{\text{eff}} = \begin{cases} 0.0121 \text{ cm}^2/\text{sec} \\ \qquad T = 550°\text{C}; P_{\text{B}} = 0.303 \text{ atm} \\ 0.0086 \text{ cm}^2/\text{sec} \\ \qquad T = 550°\text{C}; P_{\text{B}} = 0.111 \text{ atm} \end{cases}$$

The following values of the $\tilde{\phi}$ modulus,

$$\tilde{\phi} = r_p^2 \rho_p r / D_{\text{eff}} C_{\text{B}} \qquad (2)$$

ρ_p being the catalyst density and C_{B} the surface concentration of *n*-butane, were obtained:

$$\tilde{\phi} = 0.0322 \text{ (at 0.303 atm)}$$
$$\tilde{\phi} = 0.0821 \text{ (at 0.111 atm)}$$

Such values are sufficiently small to guarantee an almost unitary value of effectiveness, despite the form of the rate equation.

A general scheme of *n*-butane dehydrogenation can be written as follows:

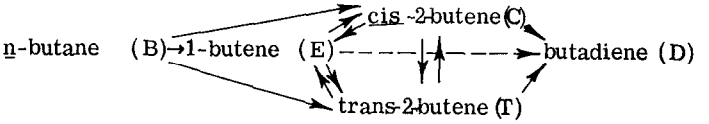

(3)

Our experimental analysis cannot give a complete account of the kinetic behavior according to such a scheme. Nevertheless some information can be derived from the comparison of mean values of the butene molar ratios, obtained from the R values of Table 3, with the corresponding equilibrium ratios. The latter have been obtained from the standard free energies of formation of the compounds (*6*). Such a comparison is reported in Table 4. It comes out that the experimental values are quite close to the calculated ones. This indicates that the distribution of butenes is largely dominated by the equilibrium conditions and therefore it is difficult to establish if one of the butenes is preferentially formed from *n*-butane. On the other hand, from the data of Table 4 it appears that the experimental ratios (C/E) and (T/E) are generally smaller than the equilibrium ones. This fact seems to indicate that 2-butenes have a slightly higher dehydrogenation rate than 1-butene.

TABLE 4
COMPARISON BETWEEN EQUILIBRIUM AND EXPERIMENTAL 2-BUTENE DISTRIBUTION RATIOS[a]

T (°C)	(C/T)		(C/E)		(T/E)	
	Equil.	Exptl.	Equil.	Exptl.	Equil.	Exptl.
550°	0.672	0.720	1.194	0.904	1.776	1.256
530°	0.669	0.743	1.261	1.104	1.883	1.486
510°	0.663	0.786	1.318	1.393	1.989	1.772

[a] The meaning of C, T, and E appears in scheme (3).

The kinetic mechanism for the *n*-butane dehydrogenation reaction was selected by analysis of the influence of the reactant partial pressure on reaction rate. The trend of the experimental data of Table 3, graphically reported in Fig. 4, suggests that the rate-determining step is the surface reaction, which involves two adjacent active centers (dual-site). The rate equation corresponding to this mechanism is

$$r = \frac{k_r b_{\text{B}} (P_{\text{B}} - P_\Delta P_{\text{H}}/K)}{(1 + b_{\text{B}} P_{\text{B}} + b_\Delta P_\Delta + b_{\text{H}} P_{\text{H}} + b_{\text{D}} P_{\text{D}})^2} \qquad (4)$$

where P_{B}, P_Δ, P_{H}, and P_{D} are the partial pressures of *n*-butane, *n*-butenes, hydrogen, and butadiene, respectively. The adsorption of nitrogen has been neglected in all the cases. The corresponding adsorption equilibrium constants are b_{B}, b_Δ, b_{H}, and b_{D}; K is the overall gas-phase equilibrium constant.

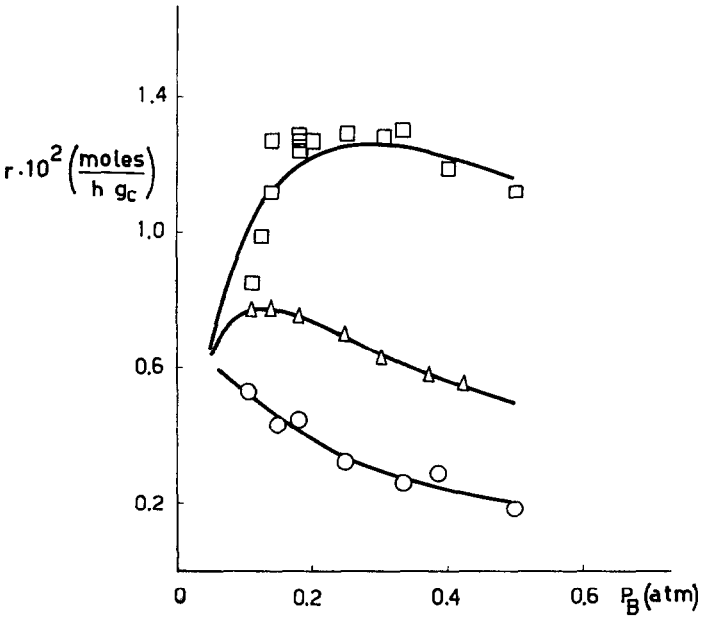

FIG. 4. Reaction rates (moles/hr g_c) vs. *n*-butane partial pressure (atm): □, 550°C; △, 530°C; ○, 510°C. Solid lines calculated from Eq. (5).

Due to our small conversion degree (about 2%) at all the investigated temperatures the reverse reaction can be neglected and besides the adsorption effects of the reaction products are reasonably small. Therefore in a first approximation the analysis of the experimental data relative to reaction rate has been made neglecting the adsorption effects of the products which are not present in the feeding mixtures. By this procedure it was possible to obtain the adsorption equilibrium constants that were successively employed for testing the validity of the previous approximation.

For feeding mixtures constituted by *n*-butane plus nitrogen, Eq. (4) becomes

$$r = \frac{k_r b_B P_B}{(1 + b_B P_B)^2} \qquad (5)$$

that can be written as follows:

$$\left(\frac{P_B}{r}\right)^{1/2} = \frac{1}{(k_r b_B)^{1/2}} + \left(\frac{b_B}{k_r}\right)^{1/2} P_B \qquad (6)$$

This is a linear relation between $(P_B/r)^{1/2}$ and P_B. Such a plot is given in Fig. 5 in which the best straight lines evaluated by the least-square method are also reported. The significance of the regression coefficients $(b_B/k_r)^{1/2}$ can be obtained applying the t test. It derives that for the lines of Fig. 5 the probabilities corresponding to the calculated t values are less than 1%. This figure corresponds (*7*, *8*) to highly significant values of the obtained regression coefficients.

From the parameters of the lines shown in Fig. 5 the values of k_r and b_B reported in Table 5 were obtained. The behavior of the reaction rate curves drawn in Fig. 4, employing such values of k_r and b_B (solid lines), reveals a satisfactory agreement between the experimental data and calculated values.

TABLE 5
REACTION RATE AND ADSORPTION EQUILIBRIUM CONSTANTS

T (°C)	$k_r \times 10^2$ (moles/hr g cat.)	b_B (atm^{-1})	b_A (atm^{-1})	b_H (atm^{-1})
510°	2.44	19.50	57.605	52.436
530°	3.11	8.00	22.10	21.796
550°	5.05	3.63	9.61	11.003

For feeding mixtures of *n*-butane, nitrogen, and a component i (1-butene or hydro-

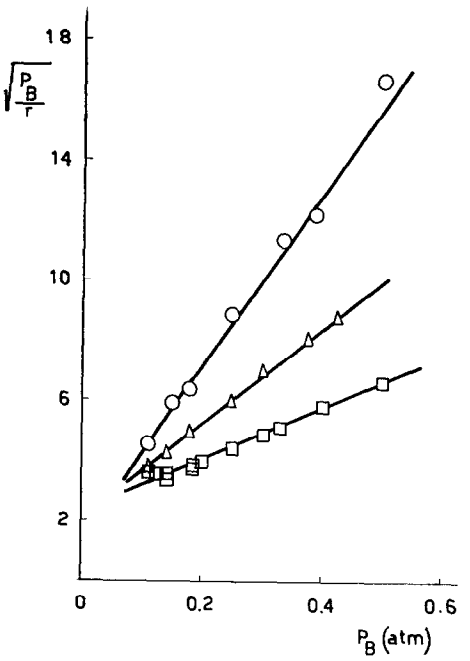

FIG. 5. $(P_B/r)^{1/2}$ as a function of *n*-butane partial pressure: □, 550°C; △, 530°C; ○, 510°C.

gen), Eq. (4), by taking into account that the partial pressure of *n*-butane was kept constant, can be written

$$r = \frac{k_r b_B (P_B - P_\Delta P_H/K)}{(1 + b_B P_B + b_i P_B R_i)^2} \qquad (7)$$

R_i being the mole ratio of the i component over *n*-butane. The previous equation can be rearranged as follows:

$$\left[\frac{(P_B - P_\Delta P_H/K)}{r}\right]^{1/2} = \frac{1 + b_B P_B}{(k_r b_B)^{1/2}} + \frac{b_i P_B}{(k_r b_B)^{1/2}} R_i \qquad (8)$$

that is a linear relationship between the first member and the ratio R_i. Such plots are reported in Figs. 6 and 7 for the runs corresponding to mixtures of *n*-butane and 1-butene and mixtures of *n*-butane and hydrogen, respectively. The application of the t test to their regression coefficients gave probability values less than 1%. Therefore it derives that also the runs performed with addition of a reaction product to the feeding mixture are consistent with the dual-site mechanism.

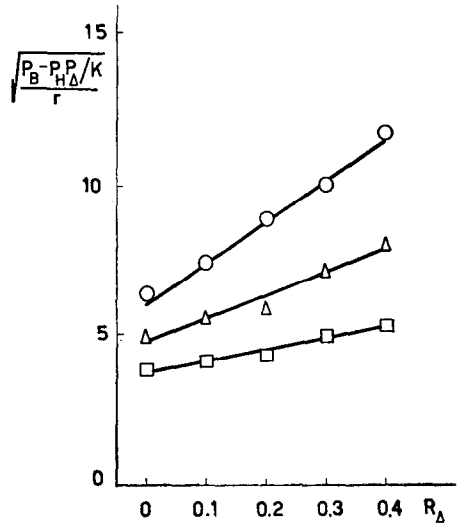

FIG. 6. $\left(\frac{P_B - P_H P_\Delta/K}{r}\right)^{1/2}$ as a function of R_Δ (1-butene/*n*-butane) molar ratio in the feeding mixtures.

From the parameters of straight lines of Figs. 6 and 7 and from the values of k_r and b_B given in Table 5 the adsorption equilibrium constants b_Δ and b_H reported in the same table were obtained. It is interesting to point out that the values of the ratios (b_H/b_Δ) (0.91, 0.99, 1.15 at the three tem-

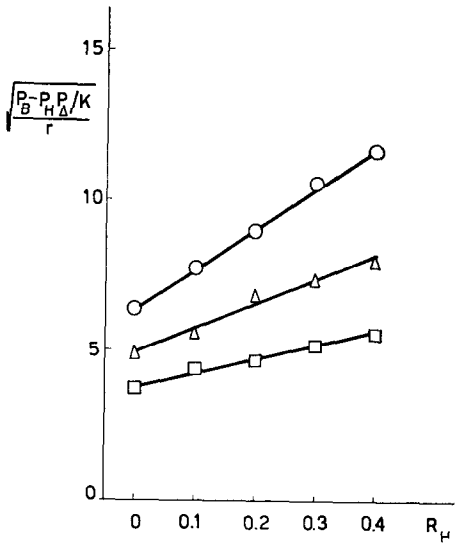

FIG. 7. $\left(\frac{P_B - P_H P_\Delta/K}{r}\right)^{1/2}$ as a function of R_H (hydrogen/*n*-butane) molar ratio in the feeding mixtures.

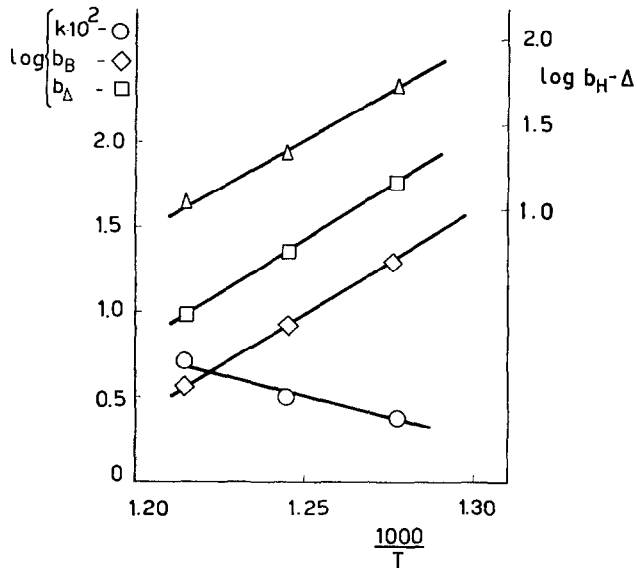

FIG. 8. Log k_r, b_B, b_Δ, b_H as a function of $10^3/T$ (data of Table 5).

peratures) are close to the value 0.82 obtained by Balandin and co-workers (*9*, *10*) in the dehydrogenation of 1-butene to butadiene at 560°C on chromia-alumina catalyst.

In Fig. 8 the plots log k_r, b_B, b_Δ, b_H vs. $(10^3/T)$ are reported. For k_r the following equation is derived:

$$\log k_r = 4.850 - 23{,}223/2.303\,RT \qquad (9)$$

From the slopes and intercepts of the other lines the standard heats and entropies of adsorption were evaluated through the equation

$$b = \exp[-(\Delta H^\circ/RT) + (\Delta S^\circ/R)] \qquad (10)$$

and the obtained values are reported in Table 6.

TABLE 6
ADSORPTION PARAMETERS

Compound	$-\Delta H^\circ$ (kcal/mole)	$-\Delta S^\circ$ (cal/mole °K)
Butane	53.90 (±0.55)	62.94 (±0.72)
Butene	57.43 (±0.84)	65.30 (±1.05)
Hydrogen	50.11 (±1.78)	56.17 (±2.24)

Employing the values of adsorption equilibrium constants collected in Table 5, it is now possible to check how good is the approximation by which the Eqs. (5) and (7) have been obtained from Eq. (4). The adsorption equilibrium constant of butadiene has been evaluated on the basis of the value 9.5 obtained by Balandin (*10*) in the dehydrogenation of 1-butene for the ratio (b_D/b_Δ). This assumption is justified by the fact that our ratio (b_H/b_Δ) is also quite close to the value reported in the same papers. Taking into account all the adsorption equilibrium constants it is derived that the correction of the reaction rate in the investigated *n*-butane partial pressure range is about 5%. The neglect of such a correction does not affect any conclusion.

As the reactions which were performed with doped catalysts, one can assume that the chemisorption constant b_B is only slightly affected by the addition of impurities. If the fact that all the reaction rates reported in Fig. 2 were measured at the same value P_B is taken into account, it follows that

$$\ln(r/r_0) = -\Delta E_a/RT \qquad (11)$$

In Eq. (11) r and r_0 are the reaction rates on doped and Type 0 catalysts, respectively; ΔE_a is the increase of activation energy on doped catalyst with respect to the Type 0 catalyst. Good straight lines of ln r vs. $(1/T)$

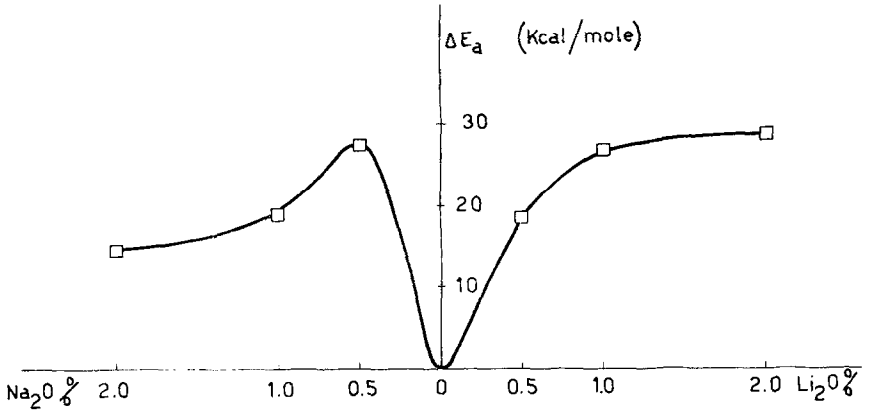

FIG. 9. ΔE_a vs. Li_2O or Na_2O percentages in the catalysts.

plots were obtained that justify the approximation of Eq. (11). The results of this analysis are reported in Fig. 9.

REACTION MECHANISM

The experimental reaction rate data confirm the validity of the Langmuir-Hinshelwood scheme for the description of the *n*-butane dehydrogenation reaction. The kinetic mechanism of the reaction reveals that the rate-determining step is the surface reaction with a dual-site mechanism. This result confirms the previous findings of Dodd and Watson (*1*).

On the other hand it is noteworthy that in the dehydrogenation of cyclohexane on the same catalysts the rate-determining step is the hydrocarbon chemisorption as it is substantiated by the absence of cyclohexene and cyclohexadiene in the reaction products (*11*). The much larger rate of the surface reaction of cyclohexane with respect to *n*-butane could be due to participation of an hexagonal array of surface chromium ions on chromia (*12*) as it is claimed in the hydrogenation of aromatic hydrocarbons.

The *n*-butane chemisorption centers on the catalyst are localized on Cr^{2+} ions (*11*, *13*). The chemisorption process occurs through a cleavage of a C—H bond; the alkyl group is bound to a Cr^{2+} ion on the catalyst surface and the H atom to one of the neighboring oxygen atoms. The bond between the alkyl group and the metal can be described as a *strong* acceptor bond, because a free electron is captured by the radical (*14*). In the language of the crystal field theory of chemisorption (*15*) this corresponds to the fulfillment of coordination of Cr(III) with formation of a surface octaedral complex.

The further step of the dehydrogenation reaction, according to the experimentally found dual-site mechanism, seems to be due to the intervention of another Cr^{2+} ion, that abstracts an hydrogen atom from the adsorbed alkyl radical. The experimentally found strong competition in chemisorption of hydrogen and *n*-butane can support this interpretation. The desorption of hydrogen and of the olefin molecules constitutes the last step of the reaction.

The formation of divalent chromium ions on the catalyst can be due to a catalyst partial reduction. Measurements of electrical conductivity of chromia-alumina catalysts as a function of temperature (*16*, *17*), showed that the catalyst is a semiconductor with amphoteric nature (*n*- or *p*-type depending on the physical conditions) and therefore both *free electrons* and *holes* are present on its surface.

In a semiconductor lattice the electron shifting is easy and it follows that the previous mechanism can be interpreted in the light of the electronic theory of catalysis (*14*, *18*, *19*).

The proposed reaction mechanism is shown in Fig. 10, where $\ominus$ and $\oplus$ indicate the electrons and the holes on the catalyst surface, respectively. If n_i indicates the surface concentration of the *i*th species,

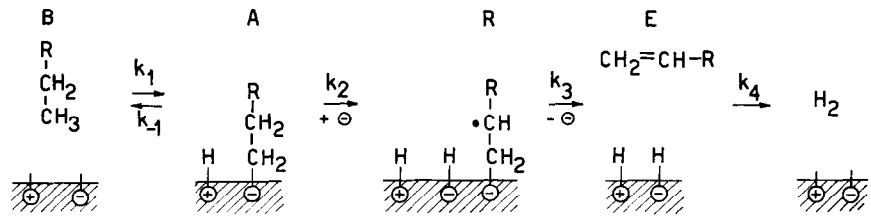

FIG. 10. Scheme of the reaction mechanism.

neglecting adsorption of reaction products and denoting by B, *n*-butane; A, R—CH_2—CH_2—; R, R—$CH^{\cdot}$—CH_2—; E, R—CH = CH_2; for low coverage, that is for $n_\ominus \gg n_A$, we obtain the following relations:

$$dn_A/dt = k_1P_B - k_{-1}n_An_{H^+} - k_2n_An_\ominus \quad (12)$$

$$dn_R/dt = k_2n_An_\ominus - k_3n_R \quad (13)$$

The meaning of the constants k_i is given in Fig. 10. At the equilibrium we have

$$k_1P_B = k_{-1}n_An_{H^+} + k_2n_An_\ominus \quad (14)$$

$$k_3n_R = k_2n_An_\ominus = r_E \quad (15)$$

r_E being the desorption rate of *n*-butane, that is the rate of the overall process. If

$$k_2n_An_\ominus \ll k_{-1}n_An_{H^+} \quad (16)$$

as is justified by the fact that the rate-determining step is the surface reaction, from Eq. (14) there derives

$$n_A = k_1P_B/k_{-1}n_{H^+} \quad (17)$$

and therefore Eq. (15) becomes

$$r_E = k_1k_2P_Bn_\ominus/k_{-1}n_{H^+} = b_Bk_2P_Bn_{\ominus/+} \quad (18)$$

For small coverages, Eq. (5) becomes $r = k_rb_BP_B$; a comparison with Eq. (18) gives

$$k_r = k_2n_\ominus/n_{H^+} \quad (19)$$

Both $n_\ominus$ and n_{H^+} depend on the position of the Fermi level μ_F of the solid and therefore also the reaction rate is affected by the value of the Fermi level. Since $n_\ominus$ increases by increasing μ_F, while it is possible to show (*14*) that the concentration of a species bound to the catalyst surface with a *strong* donor bond (H-⊕) decreases by increasing μ_F, then globally the reaction rate should follow the variation of μ_F.

The previous analysis can be useful for the interpretation of the influence of the impurities added to the catalyst on its activity. As is known, foreign atoms added to a crystalline solid can replace the regular lattice atoms (substitutive solution) or can be thrown into interstitial positions or onto the surface of the crystal. The relative concentration of impurities in reticular or interstitial position is largely dominated by the values of the impurity and host ion radii. For the system under consideration the values of ionic radii are the following (Å): Al^{3+}, 0.50; Cr^{3+}, 0.69; Li^+, 0.60; Na^+, 0.95 (*20*). From these values it derives that Li^+ ions can substitute both Cr^{3+} and Al^{3+} ions in the lattice much better than Na^+ ions. The difficulty of Na^+ ion to substitute Cr^{3+} ions, due to the higher ionic radius of the former, can hinder diffusion of sodium in the lattice during the preparation of the catalyst. Therefore in larger amounts it will tend to remain on interstitial positions at the surface of the catalyst. That means that sodium can act as an amphoteric impurity and only a small amount of Na^+ ions can occupy ion vacancies of Cr^{3+}.

A monovalent alkaline atom present in a reticular position acts as an electron acceptor, because it provides to the system only one electron, while the communal sharing system demands three (*21*). The indispensable two electrons will be extracted from the normal electronic distribution of the crystal, leaving two partially free positive holes able to wander in the neighborhood of the defect. On the other hand a monovalent largely electropositive atom in an interstitial position acts as an electron donor, giving to the system one electron.

The previous analysis seems to confirm the experimental results shown in Fig. 2; in

fact, the addition of lithium, that acts as an electron acceptor and decreases μ_F, gives at every concentration a decrease of catalyst activity. The addition of sodium gives a decrease of activity if its concentration is small and then it acts as an electron acceptor, followed by an increase of the activity at the higher concentrations, at which it acts as an electron donor. This fact seems to be confirmed by the behavior of the curve of Fig. 9, in which it can be seen that, while ΔE_a increases monotonically by addition of lithium, it goes through a maximum by addition of sodium.

ACKNOWLEDGMENT

We are indebted to the Italian Consiglio Nazionale delle Ricerche for financial aid.

REFERENCES

1. DODD, R. H., AND WATSON, K. M., *Trans. Am. Inst. Chem. Engrs.* **42,** 263 (1946).
2. HAPPEL, J., BLANCK, H., AND HAMILL, T. D., *I. & E.C. Fundamentals* **5,** 289 (1966).
3. EMMETT, P. H., ed. "Catalysis," Vol. 1, p. 343. Reinhold, New York, 1954.
4. YOSHIDA, F., RAMASWAMI, D., AND HOUGEN, O. A., *A. I. Ch. E. J.* **8,** 1, 5 (1962).
5. HIRSCHFELDER, J. O., CURTISS, C. F., AND BIRD, R. B., "Molecular Theory of Gases and Liquids." Wiley, New York, 1954.
6. "Selected Values of Physical and Thermodynamic Properties of Hydrocarbons and Related Compounds." Am. Petroleum Inst., Carnegie Press, 1953.
7. CHAN HUI CHOU, *Ind. Eng. Chem.* **50,** 799 (1958).
8. FRANCKAERTS, J., AND FROMENT, G. F., *Chem. Eng. Sci.* **19,** 807 (1954).
9. BALANDIN, A. A., BOGDANOVA, O. K., AND SHCHEGLOVA, A. P., *Izv. Akad. Nauk SSSR. Otd. Khim. Nauk.* **5,** 497 (1946).
10. BALANDIN, A. A., *Advan. Catalysis* **10,** 96 (1958).
11. VAN REIJEN, L. L., SACHTER, W. M. H., COSSEE, P., BROUWER, D. M., *Proc. Intern. Congr. Catalysis, 3rd, Amsterdam, 1964,* p. 829.
12. DAVIS, R. J., *in* "Chemisorption." Butterworths, London, 1957.
13. BURWELL, R. L., LITTLEWOOD, A. B., CARDEW, M., PASS, G., AND STODDARD, C. T. H., *J. Am. Chem. Soc.* **82,** 6272 (1960).
14. WOLKENSTEIN, T., "Théorie électronique de la catalyse sur les semiconducteurs." Masson & Cie, Paris, 1961.
15. DOWDEN, D. A., AND WELLS, D., *Actes Congr. Intern. Catalyse, 2e, Paris, 1960,* p. 1499.
16. CHAPMAN, P. R., GRIFFITH, R. H., AND MARSH, J. D. F., *Proc. Roy. Soc., London* **224,** 419 (1954).
17. WELLER, S. W., AND VOLTZ, S. E., *Advan. Catalysis* **9,** 215 (1957).
18. GARRETT, C. G. B., *J. Chem. Phys.* **33,** 966 (1960).
19. HAUFFE, K., *Advan. Catalysis* **7,** 213 (1955).
20. PAULING, L., "The Nature of the Chemical Bond," 3rd ed. Cornell Univ. Press, Ithaca, New York.
21. SUCHET, J. P., "Chemical Physics of Semiconductors." Van Nostrand, London, 1965.